Analysis of Closed Arbitrary Dielectric Waveguides Using a Modified Rayleigh–Ritz Technique

Brian Young, *Member, IEEE*

Abstract—**To avoid the meshing difficulties of the finite-element method, the classical Rayleigh–Ritz method is combined with an additional optimization to analyze closed arbitrary dielectric waveguides. The method is easily implemented in compact code and is user-friendly. The paper develops the method and its rationale and presents numerical examples to demonstrate its accuracy in propagation constant and nonperturbational loss calculations. In addition, the method is shown to be rapidly convergent and extremely stable.**

I. Introduction

VARIATIONAL expressions are known to provide a powerful basis for the solution of boundary value problems. The publication of Berk's variational formulas [1] and expositions on the theory by Collin [2] and Harrington [3] led to considerable interest in variational methods for the solution of electromagnetic boundary value problems. Early applications centered on the ability of the variational method, through the Rayleigh–Ritz technique, to provide approximate closed-form solutions for the propagation constants of inhomogeneously loaded rectangular waveguide [4], [5]. Similar applications receive continuing interest [6], [7].

The widespread availability of computers allowed numerical computation to supersede approximate analysis. The trends in variational analysis were to either increase the number of terms in the approximate analysis to converge it to the exact answer or to replace the entire-domain basis functions with an assembly of subdomain functions. The first trend, following the classical Rayleigh–Ritz technique, uses the computer to alleviate the analytical difficulty associated with increasing the number of basis functions. The second trend, generally implemented as a finite-element method, attacks the problem in a fundamentally computer-oriented approach. Both methods are theoretically capable of an exact solution. The question of which to use hinges on the relative advantages of speed, accuracy, generality, and complexity of use.

A proper implementation of the finite-element method can achieve excellent generality, high accuracy, and spurious-free solutions. However, the mesh of subdomain basis functions is critical to the method's success: the number of functions must be minimized to keep computation times reasonable while not sacrificing accuracy. In practice, a graded mesh is required, with finer meshing where field values change rapidly. In simple implementations, the user supplies the mesh details, forcing the user to be well versed in both the method and in electromagnetic theory to anticipate the field configuration. Sophisticated implementations avoid user input through automatic and adaptive mesh generation. Mesh generation techniques are difficult subjects that dramatically complicate the original simplicity of the underlying variational analysis as well as the actual computer implementation.

With its base in entire-domain basis functions, the Rayleigh–Ritz technique requires no mesh and so avoids both detailed user involvement and complicated implementations. With the same variational foundation as the finite-element method, a Rayleigh–Ritz method provides similar power in a relatively simple and user-friendly format. Relative to the finite-element method, few full-wave waveguide studies have been based on the Rayleigh–Ritz technique. Those that have appeared incorporate approximations [8], lack generality [9]–[12], or report poor performance [11]–[14].

This paper presents the first full-scale implementation of the Rayleigh–Ritz technique applied to a general full-wave frequency-dependent wave-guiding problem. The goal is to provide an analysis tool that is general, powerful, and easily and compactly implemented and that requires little input or expertise on the part of the user. The specific application is to closed arbitrary dielectric waveguides. The technique is shown to be fast and accurate while avoiding the numerical difficulties and approximations previously observed in Rayleigh–Ritz techniques. Section II covers the theory of the method, Section III discusses some implementation details, while Section IV presents numerical examples to prove the accuracy of the method. The paper concludes in Section V.

II. Theory

A suitable variational expression for the calculation of the propagation constant of a waveguide is given by [15]

$$\beta = \frac{\iint_S (\omega\epsilon \hat{E}^+ \cdot \hat{E}^- - \omega\mu \hat{H}^+ \cdot \hat{H}^- + j\hat{H}^- \cdot \nabla \times \hat{E}^+ + j\hat{E}^+ \cdot \nabla \times \hat{H}^-)\, ds}{2\iint_S \hat{E}_t \times \hat{H}_t \cdot u_z\, ds} \tag{1}$$

Manuscript received June 12, 1990; revised October 16, 1990.

The author was with the Department of Electrical Engineering, Texas A&M University, College Station, TX 77843. He is now with the Radar Systems Group, Hughes Aircraft Company, 2000 E. Imperial Highway, El Segundo, CA 90245.

IEEE Log Number 9042347.

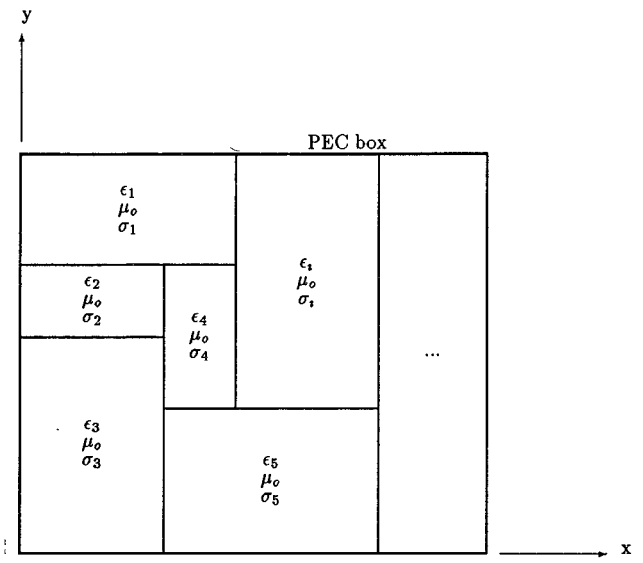

Fig. 1. Inhomogeneous rectangular waveguide with subregions.

where

$$\boldsymbol{E}^+ = \hat{\boldsymbol{E}}^+(x,y)e^{-j\beta z} = \left(\hat{\boldsymbol{E}}_t + \boldsymbol{u}_z\hat{E}_z\right)e^{-j\beta z}$$

$$\boldsymbol{H}^+ = \hat{\boldsymbol{H}}^+(x,y)e^{-j\beta z} = \left(\hat{\boldsymbol{H}}_t + \boldsymbol{u}_z\hat{H}_z\right)e^{-j\beta z}$$

$$\boldsymbol{E}^- = \hat{\boldsymbol{E}}^-(x,y)e^{j\beta z} = \left(\hat{\boldsymbol{E}}_t - \boldsymbol{u}_z\hat{E}_z\right)e^{j\beta z}$$

$$\boldsymbol{H}^- = \hat{\boldsymbol{H}}^-(x,y)e^{j\beta z} = \left(-\hat{\boldsymbol{H}}_t + \boldsymbol{u}_z\hat{H}_z\right)e^{j\beta z}.$$

This mixed-field formula requires only that $\boldsymbol{n}\times\hat{\boldsymbol{E}} = 0$ on the contour of the waveguide, a requirement that the waveguide cross section, S, be bound by a perfect electric conductor (PEC). Since this work is concerned with circuit applications rather than radiation, a closed structure is seen as closely fitting the physical reality of packaging. The formula remains stationary for the lossy case, for which $j\beta$ is replaced by $\gamma = \alpha + j\beta$. The structure is defined through inhomogeneous ϵ and μ, both of which can be complex to include loss.

The structure to which (1) is applied is shown in Fig. 1. Essentially an inhomogeneous rectangular waveguide (IRW), the structure consists of a rectangular PEC box subdivided into an arbitrary number of rectangular subregions. Each subregion is allowed a unique isotropic permittivity and conductivity. All subregions are assumed to have the permeability of free space. Note that the subregions can be placed arbitrarily as long as the entire cross section of the IRW is covered without overlaps. Structures with rectangular geometry, covering most cases of interest, can be precisely modeled. Curved and angled surfaces and graded permittivities can be modeled through staircase approximations, so fibers and novel structures can be accommodated. Considerable numerical advantage results from this system, as will be discussed below.

Suitable basis functions must be chosen for insertion into (1). The goal of this work is to minimize the effort of the user at this point. The modes of the homogeneous rectangular waveguide (HRW) of the same outer dimensions as the IRW are used as the basis functions. Note that the HRW modes form a complete set. This selection essentially expands the fields of the IRW in Fourier series. Any user with a background including Fourier series can easily grasp the basic operation of the method, freeing the user from the need of an extensive electromagnetic background. For example, doubling the width of the box will require doubling the number of basis functions to retain the same harmonic content, and hence accuracy, of the solution.

The standard E_z/H_z formulation for the HRW modes is used [16]. This choice does not lead to spurious solutions, as it does in the finite-element method, because the HRW modes are electrodynamic basis functions, meaning $\nabla\cdot\boldsymbol{H} = 0$ is explicitly satisfied throughout S. Substituting the HRW modes into (1) yields

$$\beta = \Bigg(\sum_{mn}\sum_{rs} E_{mn}E_{rs}(I_{1mnrs} + I_{2mnrs} + I_{3mnrs}) + \sum_{mn}\sum_{pq} E_{mn}H_{pq}(I_{4mnpq} + I_{5mnpq}) + \sum_{pq}\sum_{tu} H_{pq}H_{tu}(I_{6pqtu} + I_{7pqtu} + I_{8pqtu})\Bigg) \Bigg/ 2\Bigg(\sum_{mn} E_{mn}^2(I_{9mnmn} + I_{10mnmn}) + \sum_{pq} H_{pq}^2(I_{13pqpq} + I_{14pqpq})\Bigg) \tag{2}$$

where E_{mn} are the amplitudes of E_z for the TM^z modes and H_{pq} are the amplitudes of H_z for the TE^z modes. In the summations, mn and rs sum over TM^z modes, and pq and tu sum over all TE^z modes. The integral definitions appear in the Appendix.

Note that (2) applies to the general boxed IRW: the actual structure is completely defined by the integrals, which for this work are evaluated for the Fig. 1 layout. The numerical advantage of using HRW modes as bases along with rectangular subregions is that all of the integrals appearing in (2) are available in closed form. Closed-form integration provides for speed and for the precision required for numerical stability. In addition, numerical stability is enhanced since the individual HRW modes can be computed to high precision since no eigenvalue equations are involved.

To convert (2) into a matrix form suitable for computer solution, the Rayleigh–Ritz method is applied. Requiring $\partial\beta/\partial E_{mn} = 0\ \forall\ mn$ yields

$$\sum_{mn} E_{mn}(I_{1mnij} + I_{1ijmn} + I_{2mnij} + I_{2ijmn} + I_{3mnij} + I_{3ijmn}) + \sum_{pq} H_{pq}(I_{4ijpq} + I_{5ijpq}) = 4\beta E_{ij}(I_{9ijij} + I_{10ijij}) \qquad \forall\ ij = mn \tag{3}$$

and requiring $\partial\beta/\partial H_{pq} = 0\ \forall\ pq$ yields

$$\sum_{mn} E_{mn}(I_{4mnij} + I_{5mnij}) + \sum_{pq} H_{pq}(I_{6pqij} + I_{6ijpq} + I_{7pqij} + I_{7ijpq} + I_{8pqij} + I_{8ijpq}) = 4\beta H_{ij}(I_{13ijij} + I_{14ijij}) \qquad \forall\ ij = pq. \tag{4}$$

This fully dense equation is in the form of the standard eigenvalue equation. The eigenvalues are the complex propagation constants of the dominant and higher order modes of the IRW, and the eigenvectors are the TM^z and TE^z expan-

sion coefficients, which can be used to construct the IRW fields. Numerical stability is enhanced with formulation as a standard eigenvalue equation since standard routines of high stability are available.

The material filling the HRW affects the HRW mode field structures through its permittivity, ϵ_R, which directly multiplies the H_x and H_y field components but not the others. Therefore, the value of ϵ_R directly affects the relative weights of the components. A poor selection of ϵ_R will provide a poor fit to the correct field structure, yielding an inaccurate value for β. However, owing to the variational nature of the method, it is possible to optimize ϵ_R to achieve $\partial\beta/\partial\epsilon_R = 0$, as was similarly done in (3) and (4). This optimization is comparable to impedance matching the HRW to the IRW.

Since (2) is nonlinear in ϵ_R, it is not possible to lump the optimization with (3) and (4). A complex root search is necessary to find the proper value of ϵ_R such that $\partial\beta/\partial\epsilon_R = 0$. Fortunately, the derivative can be computed analytically and is numerically available in closed form, so numerical stability is not compromised. For space considerations, the derivative is not shown, but it is straightforward to derive. An extremely important consequence of the variational nature of the problem is that only one root is possible, so even though this method requires a complex root search, there is no uncertainty associated with it. When a root is found, it is the correct and only root.

The solution process then takes the following steps. After defining the structure to solve and the number of HRW modes to use, an initial guess for ϵ_R is made, perhaps automatically, and the eigenvalue problem (3) and (4) is solved. The desired mode of the waveguide is selected, for example the complex propagation constant with the largest real part to obtain the dominant mode, and $\partial\beta/\partial\epsilon_R$ is calculated. A new value of ϵ_R is then chosen and the process repeated. The iteration stops when $\partial\beta/\partial\epsilon_R = 0$.

The optimization of ϵ_R can be performed on only one eigenvalue at a time. It is possible that each eigenvalue would require reoptimization of ϵ_R, a situation that would require repeating the entire calculation for each IRW mode. However, the optimization matches the field configuration of the IRW and the expansion of HRW modes, so once matched, they describe the same waveguide, and all modes then have matched field configurations. Therefore, only one optimization is required and all eigenvalues are available with one calculation.

III. Implementation Notes

The number of HRW modes included in the solution directly determines the accuracy of the final result. Because of the Fourier series nature of the method, an accurate solution will require at least a few half-cycles of the highest-order HRW mode over the smallest feature in the IRW. This concept applies independently to the x and y directions. Given the number of half-cycles desired, N, the program can automatically determine the number of modes to include in each direction, and N would typically remain fixed for all problems but could be adjusted to check convergence. The user need not necessarily know the total number of modes utilized in the solution.

The implementation in this work allocates the TM^z_{mn} and TE^z_{pq} modes such that $m+n \leqslant L$ and $p+q \leqslant L-2$, where L is determined by N. This choice retains completeness as $L \to \infty$ while emphasizing lower-order over higher-order modes in minimizing the total number of modes.

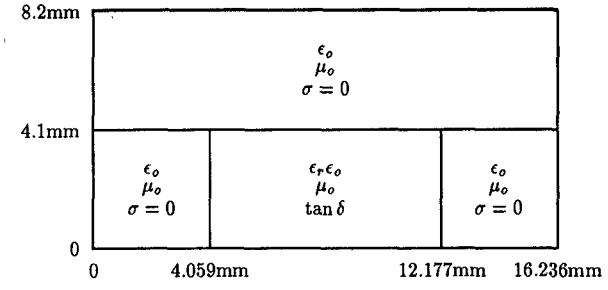

Fig. 2. Image line for numerical examples.

Structures with symmetry do not need the complete set of HRW modes, so dramatic improvements in computation speed can be achieved by deleting the appropriate modes when constructing the eigenvalue problem (3) and (4). The program need only eliminate even or odd values of m, n, p, and/or q depending on the symmetry and direction involved.

Finally, the integrations involved in (3) and (4) can be time consuming despite their calculation in closed form. However, they depend only on the IRW structure dimensions and material parameters, so they can be precomputed and stored to achieve considerable time savings. Other opportunities for precomputation exist.

IV. Results and Discussion

This section details numerical studies to prove the convergence, numerical stability, and accuracy of the Rayleigh–Ritz technique outlined in Section II. Since dominant and higher order modes are needed, symmetry is not exploited so that all modes are available with one calculation.

Convergence of the method is theoretically guaranteed. To show that convergence is actually achieved, the image line structure in Fig. 2 is computed to varying degrees of precision for two different materials, $\epsilon_r = 2.22$ and $\epsilon_r = 9.8$, with $\tan\delta = 10^{-8}$ at $B = 2.00$, where $B = f4h\sqrt{\epsilon_r - 1}/c_0$ is the normalized frequency based on the dielectric constant and height, h, of the strip. The results for the normalized propagation constants, β/β_0, of the first three modes are shown in Fig. 3. Table I shows the actual number of modes used, which also defines the order of the eigenvalue problem (3) and (4).

The results show that the method rapidly converges and that excellent numerical stability is achieved. Convergence occurs about $N = 1.5$ independent of the image line material, behavior in contrast with some previously reported dependencies [11]–[14], where convergence slows considerably for higher permittivity materials. Conceptually, dependence on the permittivity is not expected as it is the step in permittivity that requires modeling, not the step height; this can also be seen in the Fourier series expansion of a rectangular pulse, where the pulse height enters only as a scaling constant. It is interesting to note that once convergence is achieved ($N = 1.5$), increasing the number of modes by a factor of almost 4 ($N = 3$) does not introduce numerical instability. Since highly convergent and stable results with a reasonable matrix size are achieved with $N = 3$, all computed results below use

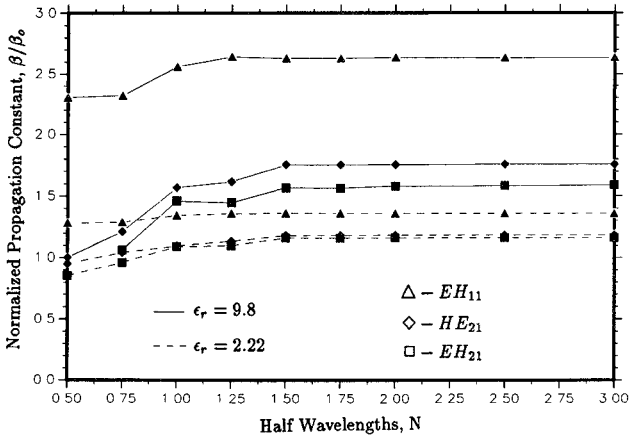

Fig. 3. Results of image line convergence study.

TABLE I
TOTAL NUMBER OF MODES FOR FIG. 3

N	No. HRW Modes
0.50	3
0.75	5
1.00	13
1.25	17
1.50	29
1.75	35
2.00	51
2.50	79
3.00	113

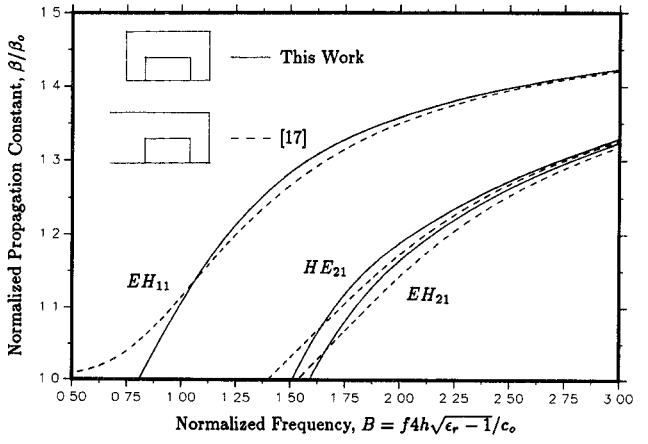

Fig. 4. Image line propagation constant comparison.

$N = 3$. This matrix size allows all data to be computed on a personal computer.

To prove the accuracy of the method for the propagation constant, the dispersion curve for the image line of Fig. 2 with $\epsilon_r = 2.22$ and $\tan\delta = 10^{-8}$ is presented. The results are shown in Fig. 4, where data from [17] are shown for comparison. The structure in [17] is open on one side, so the low-frequency behavior is necessarily different. At high frequencies, the results agree to within graphical accuracy of the [17] data. As frequency decreases, some discrepancy builds, reflecting the influence on the growing exponential tail of the extra sidewall in this work. The sidewall compresses the field, driving up the propagation constant, as

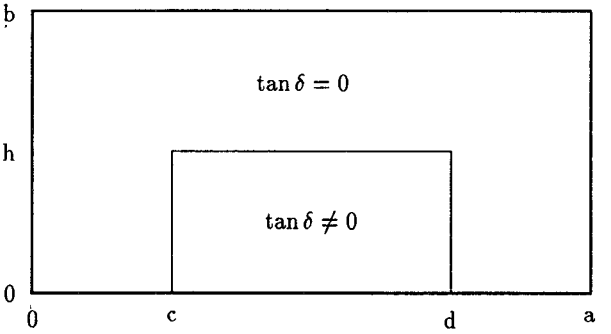

Fig. 5. Notation for perturbational loss calculation.

TABLE II
DIELECTRIC LOSS COMPARISON AT 15 GHz

	α_d, dB/m		β/β_0	
$\tan\delta$	This Work	(6)	This Work	$\sqrt{1-(\lambda_0/2a)^2}$
10^{-5}	0.007088	0.007088	0.7882	0.7882
10^{-4}	0.07088	0.07088	0.7882	0.7882
10^{-3}	0.7088	0.7088	0.7882	0.7882
10^{-2}	7.084	7.088	0.7882	0.7882
0.1	70.44	70.88	0.7887	0.7882
0.2154	150.1	152.7	0.7909	0.7882
0.4641	312.6	329.0	0.7997	0.7882
1	611.8	708.8	0.8298	0.7882

reflected in the data. At still lower frequencies, the comparison between the open and closed waveguides loses validity. The effect of the sidewall on the EH_{11} and HE_{21} modes is similar because of their similar field structures. The EH_{21} has a more complex field structure and larger evanescent tails, so the effect of the sidewall is more pronounced at all frequencies. Note that no spurious modes are observed, supporting the theoretical result.

An attenuation constant comparison is made using the image line structure of Fig. 2 with $\epsilon_r = 1$ with varying loss tangents at 15 GHz. Choosing unity dielectric constant allows for comparison with a closed-form perturbational solution. The dielectric attenuation is given by the well-known perturbational formula

$$\alpha_d = \frac{\omega \int \epsilon \tan\delta |\boldsymbol{E}|^2 \, ds}{2\,\mathrm{Re} \int \boldsymbol{E} \times \boldsymbol{H}^* \cdot \boldsymbol{u}_z \, ds} \tag{5}$$

where α_d is the dielectric attenuation constant in Np/m. Using the dimension notation from Fig. 5 and the fields of the empty waveguide TE_{10} mode ($a > b$), (5) yields

$$\alpha_d = \tan\delta \frac{k_0^2 h}{abk_z}\left(\frac{d-c}{2} + \frac{a}{4\pi}\left[\sin\left(\frac{2\pi c}{a}\right) - \sin\left(\frac{2\pi d}{a}\right)\right]\right). \tag{6}$$

The nonperturbational results using the modified Rayleigh–Ritz method are compared with the perturbational results from (6) in Table II. The results show the modified Rayleigh–Ritz technique to be very accurate in loss calculations. The deviations at higher loss tangents demonstrate the breakdown of the perturbational assumptions and the resulting loss of accuracy in (5).

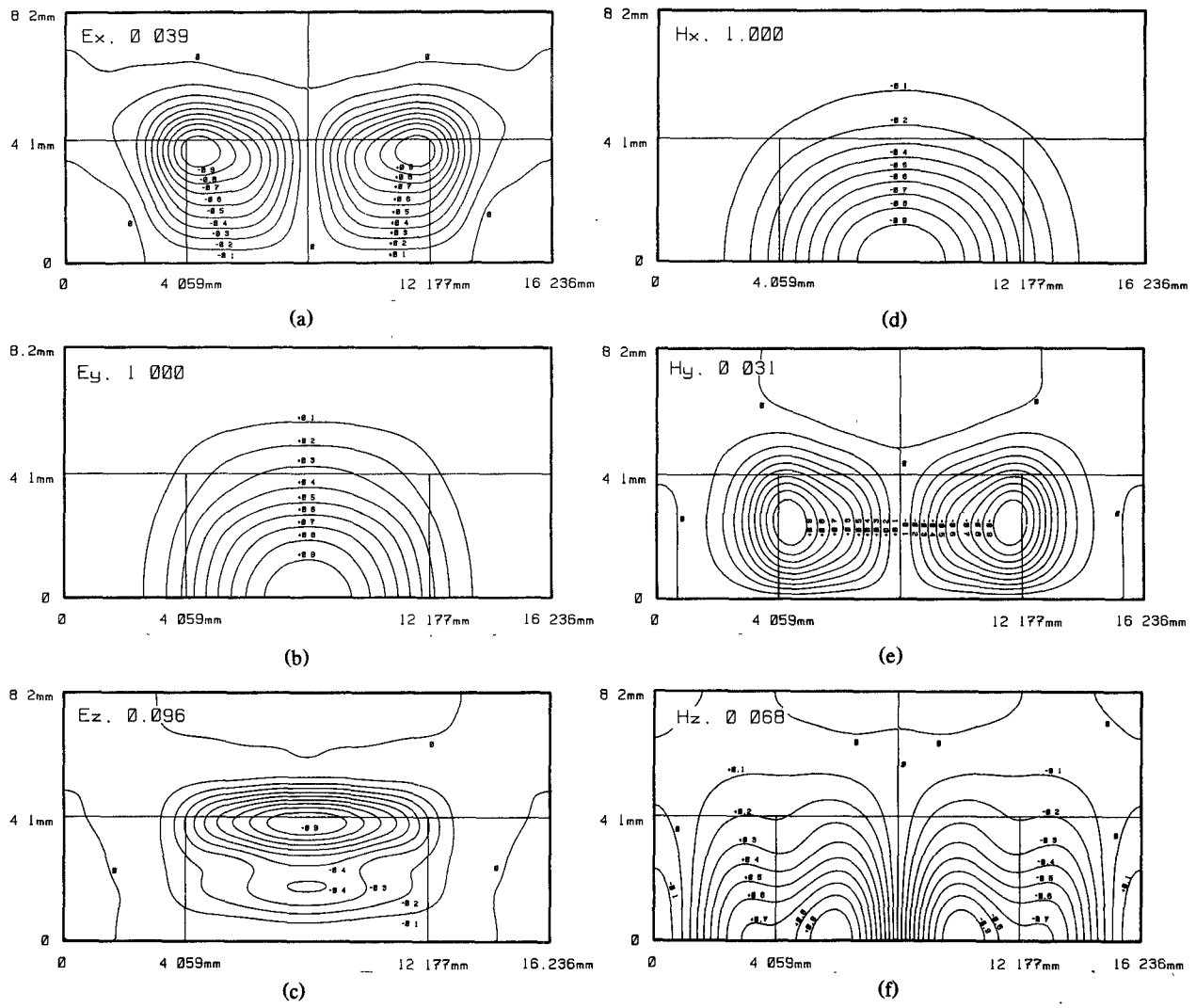

Fig. 6. Example image line field component plots.

Field plots are easily generated. An example set is shown in Fig. 6 for the dominant mode of the image line structure of Fig. 2 with $\epsilon_r = 2.22$ and $\tan\delta = 10^{-8}$ at $B = 2.25$ with $N = 4$ (199 HRW modes). At the time and distance given by $\omega t - \beta z = 0$, the real part of each component is normalized to its own peak value and then plotted as 10% contours. For the electric and magnetic fields separately, the ratio of the peak value in each component to the overall peak value is given. The relationship between all components is then fixed by the ratio of the overall peak electric and magnetic values, which is 257.10 for Fig. 6. A small amount of noise occurs in the plots because of the two-dimensional Gibbs phenomena, as indicated by the extra 0 contours. The weaker field components exhibit more noise since they are not as accurately modeled.

The field plots show strong localization of the fields to the dielectric strip and E_y and H_x component dominance. The other components primarily exist near the dielectric–air interface, especially the corners, to satisfy the boundary conditions. The dominance of the transverse components is such that the mode is almost TEM. The ratio of peak electric to magnetic field values of 257.10 corresponds closely to the 252.85 Ω intrinsic impedance of the dielectric material.

Convergence studies are usually required to determine if the PEC box is located at a sufficient distance from the guide to neglect its effect. These studies are usually time consuming to perform because of the large matrices required. A color-based graphics package has been developed that avoids the computation of contour plots in plotting the fields. The fields can be quickly computed and displayed, allowing for a visual check on the effect of the PEC walls. Coupling to the walls is readily observable and then avoided with a larger box. Since a visual check determines where coupling occurs, only the wall causing the coupling need be moved, allowing for minimization of the wall coupling with a box of minimum size.

V. Conclusion

This paper presents an alternative to the finite-element method for the general dielectric waveguide analysis problem. The method is based on the classical Rayleigh–Ritz method with an additional well-defined optimization, and it represents the first full-scale Rayleigh–Ritz implementation for waveguide analysis. Numerical results show that the method is fast, accurate, and extremely stable and well-behaved. In addition, the method is general, easily and

compactly implemented, and requires no user input beyond structure definition. The method appears to be highly suitable as the basis of a CAD system.

Appendix

The integrals appearing in (3) and (4) are given below. As written, they apply to an arbitrary isotropic IRW. For rectangular homogeneous subregions, the integrals are broken into sums of integrals over the subregions, with each integral available in closed form. The material filling the HRW is described with ϵ_R and μ_R, where ϵ_R may be complex. For this work, $\mu = \mu_R = \mu_0$:

$$I_{1mnrs} = \iint_S B_{1mnrs}\phi_{mn}\phi_{rs}\,ds$$

$$I_{2mnrs} = \iint_S B_{2mnrs}\frac{\partial\phi_{mn}}{\partial x}\frac{\partial\phi_{rs}}{\partial x}\,ds$$

$$I_{3mnrs} = \iint_S B_{3mnrs}\frac{\partial\phi_{mn}}{\partial y}\frac{\partial\phi_{rs}}{\partial y}\,ds$$

$$I_{4mnpq} = \iint_S B_{4mnpq}\frac{\partial\phi_{mn}}{\partial x}\frac{\partial\psi_{pq}}{\partial y}\,ds$$

$$I_{5mnpq} = \iint_S B_{5mnpq}\frac{\partial\phi_{mn}}{\partial y}\frac{\partial\psi_{pq}}{\partial x}\,ds$$

$$I_{6pqtu} = \iint_S B_{6pqtu}\psi_{pq}\psi_{tu}\,ds$$

$$I_{7pqtu} = \iint_S B_{7pqtu}\frac{\partial\psi_{pq}}{\partial x}\frac{\partial\psi_{tu}}{\partial x}\,ds$$

$$I_{8pqtu} = \iint_S B_{8pqtu}\frac{\partial\psi_{pq}}{\partial y}\frac{\partial\psi_{tu}}{\partial y}\,ds$$

$$I_{9mnrs} = B_{9mnrs}\iint_S \frac{\partial\phi_{mn}}{\partial x}\frac{\partial\phi_{rs}}{\partial x}\,ds$$

$$I_{10mnrs} = B_{10mnrs}\iint_S \frac{\partial\phi_{mn}}{\partial y}\frac{\partial\phi_{rs}}{\partial y}\,ds$$

$$I_{13pqtu} = B_{13pqtu}\iint_S \frac{\partial\psi_{pq}}{\partial y}\frac{\partial\psi_{tu}}{\partial y}\,ds$$

$$I_{14pqtu} = B_{14pqtu}\iint_S \frac{\partial\psi_{pq}}{\partial x}\frac{\partial\psi_{tu}}{\partial x}\,ds$$

where

$$\phi_{mn}(x,y) = \sin\left(\frac{m\pi}{a}x\right)\sin\left(\frac{n\pi}{b}y\right),$$
$$m = 1,2,3\cdots;\ n = 1,2,3,\cdots$$

$$\psi_{pq}(x,y) = \cos\left(\frac{p\pi}{a}x\right)\cos\left(\frac{q\pi}{b}y\right),$$
$$p = 0,1,2,\cdots, q = 0,1,2\cdots;\ p = q \neq 0$$

$$B_{1mnrs} = \omega(\epsilon_R - \epsilon)$$

$$B_{2mnrs} = \omega\epsilon A_{1mn}A_{1rs} + \omega\mu A_{7mn}A_{7rs} + jA_{7mn}$$

$$B_{3mnrs} = \omega\epsilon A_{3mn}A_{3rs} + \omega\mu A_{5mn}A_{5rs} + jA_{7mn}$$

$$B_{4mnpq} = 2\omega\epsilon A_{1mn}A_{2pq} + 2\omega\mu A_{7mn}A_{8pq} + jA_{1mn} + jA_{6pq}$$

$$B_{5mnpq} = 2\omega\epsilon A_{3mn}A_{4pq} + 2\omega\mu A_{5mn}A_{6pq} - jA_{1mn} - jA_{6pq}$$

$$B_{6pqtu} = \omega(\mu_R - \mu)$$

$$B_{7pqtu} = \omega\epsilon A_{4pq}A_{4tu} + \omega\mu A_{6pq}A_{6tu} + jA_{2pq}$$

$$B_{8pqtu} = \omega\epsilon A_{2pq}A_{2tu} + \omega\mu A_{8pq}A_{8tu} + jA_{2pq}$$

$$B_{9mnrs} = A_{1mn}A_{7rs}$$

$$B_{10mnrs} = -A_{3mn}A_{5rs}$$

$$B_{13pqtu} = A_{2pq}A_{8tu}$$

$$B_{14pqtu} = -A_{4pq}A_{6tu}$$

with

$$A_{1mn} = A_{3mn} = \frac{-j\beta_{mn}}{k_R^2 - \beta_{mn}^2}$$

$$A_{2pq} = -A_{4pq} = \frac{-j\omega\mu_R}{k_R^2 - \beta_{pq}^2}$$

$$A_{5mn} = -A_{7mn} = \frac{j\omega\epsilon_R}{k_R^2 - \beta_{mn}^2}$$

$$A_{6pq} = A_{8pq} = \frac{-j\beta_{pq}}{k_R^2 - \beta_{pq}^2}$$

and

$$k_R^2 = \omega^2\epsilon_R\mu_R$$

$$\beta_{ij} = \sqrt{k_R^2 - \left(\frac{i\pi}{a}\right)^2 - \left(\frac{j\pi}{b}\right)^2}.$$

Acknowledgment

Development and testing of the method were greatly aided by a substantial grant of time by the Houston Area Research Center on its SX-2 supercomputer.

References

[1] A. D. Berk, "Variational principles for electromagnetic resonators and waveguides," *IRE Trans. Antennas Propagat.*, vol. AP-4, pp. 104–111, Apr. 1956.
[2] R. E. Collin, *Field Theory of Guided Waves*. New York: McGraw-Hill, 1960.
[3] R. F. Harrington, *Field Computation by Moment Methods*. New York: Macmillan, 1968.
[4] R. H. Sheikh and M. W. Gunn, "Wave propagation in a rectangular waveguide inhomogeneously filled with semiconductors," *IEEE Trans. Microwave Theory Tech.*, vol. MTT-16, pp. 117–121, Feb. 1968.
[5] W. E. Hord and F. J. Rosenbaum, "Approximation technique for dielectric loaded waveguides," *IEEE Trans. Microwave Theory Tech.*, vol. MTT-16, pp. 228–233, Apr. 1968.
[6] S. Akiba and H. A. Haus, "Variational analysis of optical waveguides with rectangular cross section," *Appl. Opt.*, vol. 21, pp. 804–808, Mar. 1982.
[7] P. K. Mishra, A. Sharma, S. Labroo, and A. K. Ghatak, "Scalar variational analysis of single-mode waveguides with rectangular cross section," *IEEE Trans. Microwave Theory Tech.*, vol. MTT-33, pp. 282–286, Mar. 1985.
[8] T. Okoshi and K. Okamoto, "Analysis of wave propagation in inhomogeneous optical fibers using a variational method," *IEEE Trans. Microwave Theory Tech.*, vol. MTT-22, pp. 938–945, Nov. 1974.

[9] J. B. Davies, "Propagation in rectangular waveguide filled with skew uniaxial dielectric," *IEEE Trans. Microwave Theory Tech.*, vol. MTT-15, pp. 372–376, June 1967.
[10] W. J. English, "Vector variational solutions of inhomogeneously loaded cylindrical waveguide structures," *IEEE Trans. Microwave Theory Tech.*, vol. MTT-19, pp. 9–18, Jan. 1971.
[11] S. Halevy, S. Raz, and H. Cory, "Bandwidth optimization by dielectric loading," *IEEE Trans. Microwave Theory Tech.*, vol. MTT-26, pp. 406–412, June 1978.
[12] C.-T. Liu and C. H. Chen, "A variational theory for wave propagation in inhomogeneous dielectric slab loaded waveguides," *IEEE Trans. Microwave Theory Tech.*, vol. MTT-29, pp. 805–812, Aug. 1981.
[13] A. Vander Vorst and R. Govaerts, "On the accuracy obtained when using variational techniques for asymmetrically loaded waveguides," *IEEE Trans. Microwave Theory Tech.*, vol. MTT-17, pp. 51–52, Jan. 1969.
[14] A. S. Vander Vorst, A. A. Laloux, and R. J. M. Govaerts, "A computer optimization of the Rayleigh–Ritz method," *IEEE Trans. Microwave Theory Tech.*, vol. MTT-17, pp. 454–460, Aug. 1969.
[15] R. F. Harrington, *Time Harmonic Electromagnetic Fields*. New York: McGraw-Hill, 1961, p. 347.
[16] S. Ramo, J. Whinnery, and T. Van Duzer, *Fields and Waves in Communication Electronics*. New York: Wiley, 1984, ch. 8.
[17] K. Solbach and I. Wolff, "The electromagnetic fields and the phase constants of dielectric image lines," *IEEE Trans. Microwave Theory Tech.*, vol. MTT-26, pp. 266–274, Apr. 1978.

✠

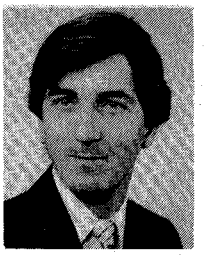

Brian Young (S'85–M'88) was born in Dallas, TX, on November 21, 1961. He received the B.S. degree from Texas A&M University in 1984, the M.S. degree from the University of Illinois at Champaign/Urbana in 1985, and the Ph.D. degree from the University of Texas at Austin in 1987, all in electrical engineering.

In 1988, he joined Texas A&M University as an Assistant Professor. In 1991 he joined the Solid-State Microwave Department of the Radar Systems Group, Hughes Aircraft Company, El Segundo, CA. His research interests are in numerical waveguide analysis, microwave/millimeter-wave/optical waveguides, electromagnetic theory, and computer-aided design.